ASCA Detection of Pulsed X-ray Emission from PSR J0631+1036

Ken'ichi Torii[1], Y. Saito[2], F. Nagase[2], T. Yamagami[2],
T. Kamae[3], M. Hirayama[4], N. Kawai[1,5,6], I. Sakurai[1], M. Namiki[1], S. Shibata[7], S. Gunji[7],
and J.P. Finley[8]

Received _____; accepted _____

[1]Cosmic Radiation Laboratory, Institute of Physical and Chemical Research (RIKEN), 2-1, Hirosawa, Wako, Saitama, 351-0198, Japan

[2]Institute of Space and Astronautical Science, 3-1-1 Yoshinodai, Sagamihara, Kanagawa, 229-8510, Japan; saito@balloon.isas.ac.jp

[3]Graduate School of Science, Hiroshima University, 1-3-1 Kagamiyama, Higashihiroshima, 739-8526, Japan; torii@crab.riken.go.jp

[4]Santa Cruz Institute for Particle Physics, University of California at Santa Cruz, Santa Cruz, CA 95064, USA

[5] Space Utilization Research Program (SURP), Tsukuba Space Center (TKSC), National Space Development Agency of Japan (NASDA), 2-1-1 Sengen, Tsukuba, Ibaraki, 305-8505, Japan

[6]Department of Physics, Tokyo Institute of Technology, 2-12-1 Ookayama, Meguro-ku, Tokyo, 152-8551

[7]Department of Physics, Yamagata University, 1-4-12 Kojirakawa, Yamagata, 990-8560, Japan

[8]Department of Physics, Purdue University, West Lafayette, IN 47907, USA

ABSTRACT

ASCA's long look at the 288 millisecond radio pulsar, PSR J0631+1036, reveals coherent X-ray pulsation from this source for the first time. The source was first detected in the serendipitous *Einstein* observation and later identified as a radio pulsar. Possible pulsation in the gamma-ray band has been detected from the *CGRO* EGRET data (Zepka, et al. 1996). The X-ray spectrum in the *ASCA* band is characterized by a hard power-law type emission with a photon index $\simeq 2.3$, when fitted with a single power-law function modified with absorption. An additional blackbody component of $kT \simeq 0.14$ keV increases the quality of the spectral fit. The observed X-ray flux is $2.1 \times 10^{-13}\,\mathrm{ergs\,s^{-1}\,cm^{-2}}$ in the 1-10 keV band. We find that many characteristics of PSR J0631+1036 are similar to those of middle-aged gamma-ray pulsars such as PSR B1055-52, PSR B0633+17 (Geminga), and PSR B0656+14.

Subject headings: pulsars: general — pulsars: individual (PSR J0631+1036) — X-rays: stars: neutron

1. Introduction

Studies of rotation powered pulsars in the X-ray band give us information of their evolution of magnetospheric activities, surface temperatures, and interaction of the pulsar wind with the surrounding medium (e.g., Becker & Trümper 1997; Saito 1998). The most energetic Crab-like pulsars with the spin-down power of $\dot{E} \gtrsim 10^{37}\,\mathrm{ergs\,s^{-1}}$ show X-ray pulsations of magnetospheric origin. Most of them are associated with a supernova remnant and power synchrotron nebulae as a result of shock interaction of the pulsar wind with the ambient medium. The Vela-like pulsars, characterized by their spin-down power of $10^{36}\mathrm{ergs\,s^{-1}} \lesssim \dot{E} \lesssim 10^{37}\mathrm{ergs\,s^{-1}}$, are embedded in the extended synchrotron nebulae which often makes it difficult to study the neutron star itself. Older and weaker ($10^{34}\mathrm{ergs\,s^{-1}} \lesssim \dot{E} \lesssim 10^{35}\mathrm{ergs\,s^{-1}}$) sources show pulsating blackbody-type spectra below $\simeq 0.5 - 0.6$ keV, as well as the pulsating power-law type spectra in the hard energy band. Typical objects of this class are the three Musketeers, PSR B1055-52, PSR B0656+14, and PSR B0633+17 (Geminga) (e.g., Finley, Ögelman, & Kiziloğlu 1992; Greiveldinger, et al. 1996; Becker, et al. 1999). Interestingly, these middle-aged ($\tau \simeq 10^5 - 10^6$ yrs) pulsars convert their spin-down power into high energy γ-ray photons with higher efficiency than in younger pulsars (e.g., Thompson 1996; Kifune 1996)

The source studied herein, PSR J0631+1036, was discovered by the targeted searches for radio pulsars in unidentified *Einstein* X-ray sources (Zepka, et al. 1996). The pulse period, $P \simeq 0.288$ s, and its derivative, $\dot{P} \simeq 1.0 \times 10^{-13}\,\mathrm{s\,s^{-1}}$, give the characteristic age of $\tau = P/(2\dot{P}) = 4.3 \times 10^4$ yrs. The spin-down power is $\dot{E} = 5.4 \times 10^{34}\, I_{45}\,\mathrm{ergs\,s^{-1}}$ where I_{45} is the moment of inertia of the neutron star normalized to $10^{45}\,\mathrm{g\,cm^2}$. This range of parameters is between the Vela-like pulsars and the three Musketeers.

In the *Einstein* IPC data, about 50 photons were detected from the X-ray counterpart of the radio pulsar PSR J0631+1036. The spectral fit gave a blackbody temperature of $kT = 0.27 \pm 0.08$ keV, an absorption column $N_H = (9 \pm 4) \times 10^{21}\,\mathrm{cm^{-2}}$, and an observed X-ray flux $F_X = 1.9 \times 10^{-13}\,\mathrm{ergs\,s^{-1}\,cm^{-2}}$ in the $0.16 - 3.5$ keV band (Zepka, et al. 1996). Unfortunately, the source was located on the support rib of the IPC field. This made the source position and source spectra rather uncertain. Later, the source was serendipitously observed in the field of view of *ROSAT* PSPC. Spectral analysis gave a best-fit blackbody temperature $kT = 0.18 \pm 0.08$ keV, an absorption column $N_H = (1.2 \pm 0.6) \times 10^{21}\,\mathrm{cm^{-2}}$, and an effective radius of the emitting region of approximately $R_{\mathrm{BB}} \simeq 1$ km (Zepka, et al. 1996). Again, the source was unfortunately shadowed by the detector supporting ribs, making the obtained spectral parameters rather uncertain.

Interestingly, it was found that this source might be pulsating in the γ-ray energy band. Zepka, et al. (1996) folded the arrival times of 267 counts from *CGRO* EGRET at the expected pulse period. They found that the folded light curve was significantly displaced from uniform distribution at more than 99 % confidence.

2. Observation

We have proposed and carried out the *ASCA* observation of PSR J0631+1036 during 1998, October 16-18. *ASCA* (Tanaka, Inoue, & Holt, 1994) carries two kinds of X-ray detectors at the foci of four identical X-ray telescopes. The X-ray CCD camera, SIS (Solid-state Imaging Spectrometer; Burke, et al. 1994), has the higher energy resolution and relatively high detection efficiency in the soft energy band. The time resolution of SIS is 4-16 s in the standard mode which is not suitable for timing observation of fast pulsars. The imaging gas-scintillation proportional counter, GIS (Gas Imaging Spectrometer; Ohashi, et al. 1996; Makishima, et al. 1996), has relatively high detection efficiency in the hard energy band and high time resolution. We operated the SIS in 1-CCD faint mode with 4-s time resolution. Therefore, only pulse phase averaged spectroscopy could be made with the SIS. We operated the GIS in the PH mode and assigned a part of the telemetry bit to increase the time resolution reducing the spectral information. The resultant time resolution was 3.9 ms or better depending on the telemetry rate. We used screened event data according to the standard REV2 processing (Pier 1997). The effective exposure time was 69.6 and 76.1 ks for each SIS and GIS, respectively, and the net time span of observation was $T = 160$ ks.

3. Analysis

3.1. Timing

We analyzed the GIS data to search for pulsations in the X-ray band. The GIS observation began at 51103.0185 MJD and ended at 51104.8260 MJD. The data from GIS2 and GIS3 were co-added, yielding $\simeq$ 1100 events within $3'$ radius circular region in the total energy band of 0.7-7 keV, including background. The photon arrival times were barycentered and z_1^2 test (Buccheri, et al. 1983) and epoch folding search (e.g., Leahy, et al. 1983) were applied bracketing the expected period, $P_{\rm exp} = 0.2877671$ s at MJD 51103.9305 (middle time of the current *ASCA* observation at barycenter), from the radio ephemeris effective during the current observation (Nice 2000, private communication).

Figure 1a shows the result of z_1^2 test. We can clearly see a peak at the expected pulse period. No similar peaks have been found in the background data with better statistics extracted from the same observation. We then applied the epoch folding search. The events were folded into 6 bins and χ^2 values were calculated from each trial period. A significant peak is found (Figure 1b) at the period consistent with that obtained from the z_1^2 test. The probabilities to find higher peaks out of random fluctuations with a single trial are as low as 1.8×10^{-6} for z_1^2 test and 1.1×10^{-6} for folding search. Considering the reasonable number of independent trials ($\simeq 18$) as discussed below, the chance probabilities to find higher peaks are 3.2×10^{-5} for the z_1^2 test and 2.0×10^{-5} for the folding search. Therefore, we conclude that we have significantly detected X-ray pulsations from PSR J0631+1036 for the first time.

The pulse period is determined from folding search to be $P = 0.2877672(1)$ s at MJD 51103.9305. Here, the value in parenthesis is a 90 % confidence error to the last digit. We estimated this error by using the method of Leahy (1987), which gave tighter constraint than the nominal error of $P^2/(2T) = 3 \times 10^{-7}$ s.

The detected pulse period is consistent with the effective radio ephemeris while it is significantly shorter than the period, $P = 0.2877676$ s, which is extrapolated from the previous radio ephemeris (Zepka, et al. 1996) by $\Delta P = -4 \times 10^{-7}$ s. This difference in period may not be ascribed to a finite value of negative $\ddot{P}$, since the corresponding value of $\ddot{P} \simeq -3 \times 10^{-23}\,\mathrm{s}^{-1}$ gives an unreasonably large braking index, $n \simeq 7 \times 10^2$. Although it is not known if PSR J0631+1036 has recently glitched or not due to lack of published results (e.g., Johnston & Galloway 1999), we consider that the value of $\Delta P/P = -1.4 \times 10^{-6}$ is naturally interpreted as the result of glitch activity. The reasonable number of independent trials for the current timing analysis is then estimated by considering a large glitch of $|\Delta P/P| \lesssim 10^{-5}$ during the 4.3 years between the last published radio observation (Zepka, et al. 1996) and the *ASCA* observation. The largest glitch ever observed would fall within the range considered here (Wang, et al. 2000). Then the number of independent Fourier bins covering the period range, $P_{\rm exp} - |\Delta P_{\rm exp}| < P < P_{\rm exp} + |\Delta P_{\rm exp}|$, is 18.

The top panel of figure 2 shows the folded light curves in the total energy band. The pulse shape is singly peaked and sinusoidal. The pulse amplitude is 45 ± 16 % of the source flux excluding background. Comparison has been made of pulse profiles in different energy bands. The pulse amplitudes, derived by fitting the profiles with a sinusoidal curve, are $31\ ^{+12}_{-17}$ % and 63 ± 18 % in 0.7-1.9 and 1.9-7 keV band, respectively.

3.2. Spectrum

We analyzed the pulse phase averaged spectra by using both the SIS and GIS data. Spectra were extracted from circular regions of $3'$ radius. Background was subtracted from the same observation. For the SIS, events from the whole chip excluding the circular region of $4'$ radius around the source were used as background. For the GIS, events from circular regions of $7.5'$ radius to the north-east of the source were used as background.

A single power-law function with soft X-ray absorption was first applied for spectrum from each detector. This simple model gave acceptable fit to each data set and the spectral parameters were found to be consistent with each other within statistical errors. Therefore, we simultaneously fit the two SIS and two GIS spectra. In the fitting procedure, each data point was weighted according to the statistics (number of photons in each bin) taking into account the propagation of error due to background subtraction. For clarity, figure 3 shows the representative spectra and the best-fit model function for the two detectors (SIS1 and GIS3). The best-fit parameters are the power-law photon index, $\gamma = 2.3\ ^{+0.5}_{-0.4}$, the absorbing hydrogen column density, $N_H = (0.2\ ^{+0.2}_{-0.1}) \times 10^{22}$ cm^{-2}, and the normalization, $7\ ^{+3}_{-2} \times 10^{-5}$ photons keV^{-1} s^{-1} cm^{-2} at 1 keV with χ^2/dof=140.6/112. These errors are at one parameter 90% confidence. The observed flux is $f_X = 1.9 \times 10^{-13}\,\mathrm{ergs\,s^{-1}\,cm^{-2}}$ and the intrinsic flux is $f_X = 2.0 \times 10^{-13}\,\mathrm{ergs\,s^{-1}\,cm^{-2}}$, corresponding to the luminosity of $L_X = 2.4 \times 10^{31}\, d_1^2\, \Omega_{4\pi}\,\mathrm{ergs\,s^{-1}}$, all in 1-10 keV range. Here, d_1 is the source distance normalized to 1 kpc and $\Omega_{4\pi}$ is the emitting solid angle normalized to 4π steradian. A single blackbody model with absorption gave the best-fit temperature of $kT = 0.43$ keV while the fit was not acceptable with χ^2/dof=178.9/112.

Since the soft X-ray emission was well fit by a blackbody model (Zepka, et al. 1996), we tried blackbody plus power-law model, modified by a single absorption component. When the blackbody temperature and the normalization were fixed at the best-fit parameters derived from *ROSAT* PSPC, $kT = 0.18$ keV and $R_{\rm BB} = 1$ km at 1 kpc, the following parameters are obtained. The power-law photon index, $\gamma = 1.2 \pm 0.4$, the normalization for the power-law component $Norm = 2.1\ ^{+1.4}_{-0.9} \times 10^{-5}\,\mathrm{photons\,keV^{-1}\,s^{-1}\,cm^{-2}}$ at 1 keV and the absorption column $N_H = 0.96\ ^{+0.08}_{-0.07} \times 10^{22}\,\mathrm{cm^{-2}}$. In this case, crossover of the two components occurs at around 1.9 keV. The quality of the fit is slightly worse than the single power-law model, $\chi^2/dof = 147.1/112$. When the emitting radius of blackbody is set free, $R_{\rm BB} = (0.6\ ^{+0.1}_{-0.2})\, d_1$ km is obtained with $\gamma = 1.7 \pm 0.4$, $Norm = (4\ ^{+2}_{-1}) \times 10^{-5}\,\mathrm{photons\,keV^{-1}\,s^{-1}\,cm^{-2}}$, $N_H = 0.5 \pm 0.2 \times 10^{22}\,\mathrm{cm^{-2}}$, and $\chi^2/dof = 128.2/111$.

Starting with the best-fit parameters for the blackbody component obtained from *ROSAT*, we tried to set all the five parameters free in the two component (blackbody plus power-law) model. However, the parameters could not be well constrained due to trade-offs between the two continuum components and the arbitrary absorption column. Therefore, we fixed the temperature at a value in the range $0.1\,\mathrm{keV} \leq kT \leq 0.3\,\mathrm{keV}$ with every 0.01 keV step. Then the minimum of $\chi^2/dof = 126.1/111$, was obtained with $kT = 0.14$ keV and $R_{\rm BB} = (2.1\ ^{+0.5}_{-0.6})\,d_1$ km. The χ^2 value with $kT = 0.14$ keV is thus smallest and we consider this model is most suitable for the current *ASCA* data. The other spectral parameters for $kT = 0.14\,\mathrm{keV}$ are the power-law photon index, $\gamma = 1.9 \pm 0.4$, the normalization for the power-law component $6\ ^{+3}_{-2} \times 10^{-5}\,\mathrm{photons\,keV^{-1}\,s^{-1}\,cm^{-2}}$ at 1 keV and the absorption column $N_H = (0.8 \pm 0.2) \times 10^{22}\,\mathrm{cm^{-2}}$. With this model, the total observed X-ray flux is $f_X = 2.1 \times 10^{-13}\,\mathrm{ergs\,s^{-1}\,cm^{-2}}$ and the intrinsic flux is $f_X = 3.5 \times 10^{-13}\,\mathrm{ergs\,s^{-1}\,cm^{-2}}$ in the 1-10 keV band. The corresponding luminosity is $4.2 \times 10^{31}\,d_1^2\,\Omega_{4\pi}\,\mathrm{ergs\,s^{-1}}$. The blackbody component contributes 16 % and 34 % of the observed and intrinsic flux, respectively.

We then examined the pulse phase dependence of spectral shape by using the GIS data. We divided the data into two subsets, pulse on (high intensity) phase and pulse off (low intensity) phase. The two phases are split at phase 0.0625 and 0.5625 in figure 2. Since the statistics are limited, we fixed the absorption column at the best-fit value obtained from a single power-law model and fit the spectra with a single power-law function. The photon indices were $\gamma = 2.5\ ^{+0.7}_{-0.5}$ and $\gamma = 3.5\ ^{+1.0}_{-0.9}$ for pulse on and off phases, respectively. Although harder spectrum is suggested for higher flux phase, the photon indices are consistent within statistical errors.

4. Discussion

The overall properties of the multi-wavelength spectrum of PSR J0631+1036 from radio to X-ray and γ-ray are similar to those of other γ-ray pulsars (Thompson 1996). They are radiating a large fraction ($\gtrsim 0.1$) of their spin-down power in the γ-ray band. The X-ray luminosity, $L_X = 4.2 \times 10^{31}\,d_1^2\,\Omega_{4\pi}\,\mathrm{ergs\,s^{-1}}$, obtained from the two component spectral fit, is $\simeq 0.08\,d_1^2\,\Omega_{4\pi}\,I_{45}^{-1}$ % of the spin-down power, which is comparable to those of Vela pulsar and the three Musketeers (e.g., Saito 1998). For PSR J0631+1036 the power-law photon index which smoothly connects the X-ray and γ-ray flux is $\gamma \simeq 1.2$. Therefore, the simple extension of the X-ray spectrum with the photon index, $\gamma = 1.9 \pm 0.4$, obtained from the best power-law plus blackbody model, predicts lower γ-ray flux than observed. This situation may be reconciled with

complete pulse phase spectroscopy including appropriate blackbody model, which should be done in future observations.

The observed pulse fraction, 45 % in the 0.7-7 keV band, is comparable with $\simeq$ 40 % found for PSR B1055-52 above 1 keV (Ögelman & Finley 1993; Figure 1b) and $\simeq$ 55 % found for Geminga in 1-4 keV band (Halpern & Wang 1997). While these values are significantly larger than the pulse fraction of 14 ± 2 % for PSR B0656+14 as measured by *ROSAT* (Finley, et al. 1992). This might be partly due to the energy dependent pulse fraction of PSR B0656+14.

The significant difference between the detected and extrapolated pulse period may be understood as a result of glitch activity. Urama & Okeke (1999) have found that there exists a good correlation between young pulsars' spin-down rate and glitch activity. They predict the interval between Vela-size glitches of average $\Delta P/P = -2 \times 10^{-6}$ to be 7 years for PSR J0631+1036. In terms of the glitch activity parameter A_g, the mean fractional change in period per year owing to glitches, the predicted value is $A_g = 3.09 \times 10^{-7}\,\mathrm{yr}^{-1}$ (Urama & Okeke 1999). This corresponds to the accumulated period change during the 4.3 yrs of $\Sigma(\Delta P/P) \simeq -1.3 \times 10^{-6}$. These predictions are in good agreement with those observed, $A_g = 3.2 \times 10^{-7}\,\mathrm{yr}^{-1}$ or $\Sigma(\Delta P/P) = -1.4 \times 10^{-6}$.

On the other hand, Lyne, Shemar, & Graham-Smith (2000) studied the statistical properties of pulsar glitches by using well-defined sample and found a strong indication that pulsars with large magnetic fields suffer many small glitches while others show a smaller number of large glitches. Comparing the period and its derivative for PSR J0631+1036 with those in their sample, PSR B1758-23, possibly associated with the supernova remnant W28 (Kaspi, et al. 1993), has similar range of parameters. Therefore, PSR J0631+1036 might have experienced a large number of medium size ($\Delta P/P \simeq -10^{-7}$) glitches as in the case of PSR B1758-23. Lyne et al. (2000) also found a good correlation between $\dot{\nu}$ and the glitch spin-up rate, $\dot{\nu}_{\mathrm{glitch}}$, defined as the cumulative effect of glitch upon the frequency derivative. The relation, $\dot{\nu}_{\mathrm{glitch}} = -0.017\dot{\nu}$, leads to $\Delta P = -2.4 \times 10^{-7}$ s for PSR J0631+1036 during the time span of 4.3 yrs, in reasonable agreement with that observed, $\Delta P = -4 \times 10^{-7}$ s.

PSR J0631+1036 was first detected in the soft X-ray band, since it is in the direction of the Galactic anti-center (l, b)=(201°.22, 0°.45) where the interstellar absorption is much smaller than in the Galactic plane toward the Galactic center. Also, the detection of pulsed X-ray emission could be made only with long exposure time as performed with *ASCA* referring to the previously known radio period. This lesson suggests that there may be other similar sources hidden in the Galactic plane. Combined analyses of radio,

X-ray, and unidentified γ-ray sources may be useful (e.g., Roberts, Romani, & Kawai 2001).

In summary, we have detected the pulsed X-ray emission from PSR J0631+1036 for the first time. The negative offset of the observed period from the extrapolated radio ephemeris is attributable to the accumulated change in period due to glitch activity. The X-ray spectrum is well described by a power-law plus blackbody model with observed flux $f_X = 2.1 \times 10^{-13}\,\mathrm{ergs\,s^{-1}\,cm^{-2}}$ in the 1-10 keV band.

Acknowledgments — The authors would thank David Nice for providing us with the radio ephemeris of PSR J0631+1036 prior to publication. The authors are grateful to all the members of the *ASCA* team for making the observation possible.

REFERENCES

Becker, W., & Trümper, J. 1997, A&A, 326, 682

Becker, W., Kawai, N., Brinkmann, W., & Mignani, R. 1999, A&A, 352, 532

Buccheri, R., et al. 1983, A&A, 128, 245

Burke, B.E., Mountain, R.W., Daniels, P.J., Cooper, M.J., & Dolat, V.S. 1994, IEEE Trans. Nuclear Science 41, 375

Finley, J.P., Ögelman, H., & Kiziloğlu, Ü. 1992, ApJ, 394, L21

Greiveldinger, C., et al. 1996, ApJ, 465, L35

Halpern, J.P., & Wang, F.Y.-H. 1997, ApJ, 477, 905

Johnston, S., & Galloway, D. 1999, MNRAS, 306, L50

Kaspi, V.M., Lyne, A.G., Manchester, R.N. Johnston, S., D'Amico, N., & Shemar, S.L. 1993, ApJ, 409, L57

Kifune, T. 1996, Pulsars: Problems & Progress ASP Conference Series, Vol. 105, eds. S. Johnston, M.A. Walker, & M. Bailes, P.339

Leahy, D.A., Darbro, W., Elsner, R.F., Weisskopf, M.C., Kahn, S., Sutherland, P.G., & Grindlay, J.E. 1983, ApJ, 266, 160

Leahy, D.A. 1987, A&A, 180, 275

Lyne, A.G., Shemar, S.L., & Graham-Smith, F. 2000, MNRAS, 315, 534

Makishima K., et al. 1996, PASJ, 48, 171

Ögelman, H., & Finley, J.P. 1993, ApJ, 413, L31

Ohashi, T., et al. 1996, PASJ, 48, 157

Pier, E.A. 1997, ASCA getting started guide for revision 2 data, version 6.1 (available at ftp://legacy.gsfc.nasa.gov/asca/doc/)

Roberts, M.S.E., Romani, R.W., & Kawai, N. 2001, ApJ, submitted

Saito, Y. 1998, Doctor thesis, University of Tokyo (ISAS Research Note 643)

Tanaka, Y., Inoue, H., & Holt, S.S. 1994, PASJ, 46, L37

Taylor, J.H., & Cordes, J.M. 1993, ApJ, 411, 674

Thompson, D.J. 1996, Pulsars: Problems & Progress ASP Conference Series, Vol. 105, eds. S. Johnston, M.A. Walker, & M. Bailes, P.307

Urama, J.O., & Okeke, P.N. 1999, MNRAS, 310, 313

Wang, N., Manchester, R.N., Pace, R.T., Bailes, M., Kaspi, V.M., Stappers, B.W., & Lyne, A.G. 2000, MNRAS, 317, 843

Zepka, A., Cordes, J.M., Wasserman, I., & Lundgren, S.C. 1996, ApJ, 456, 305

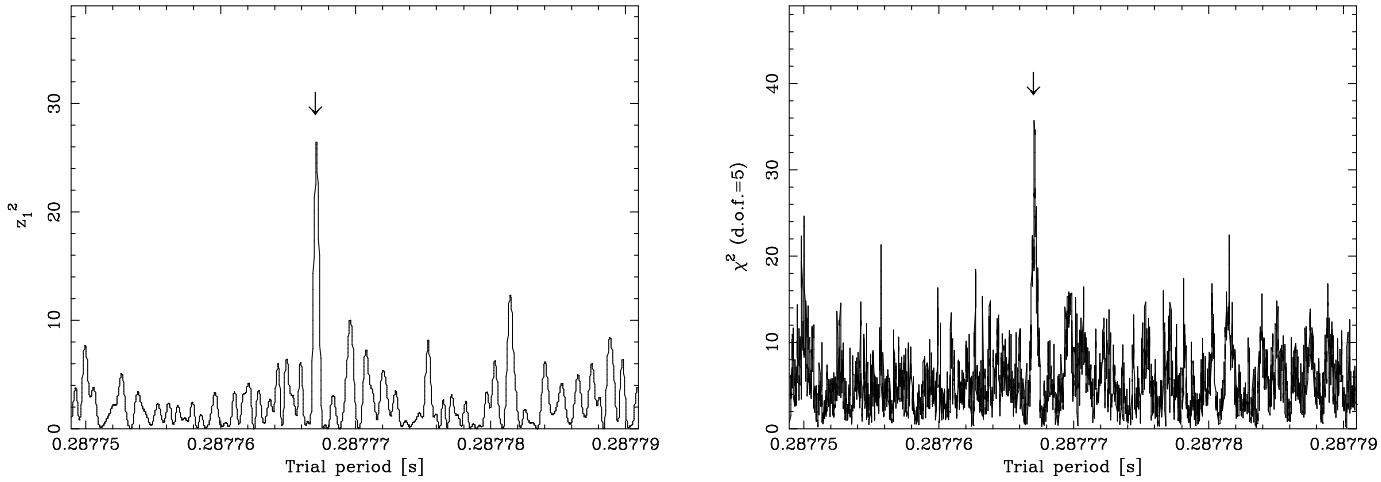

Fig. 1.— The z_1^2 and χ^2 are plotted as a function of trial periods. Arrows show the expected period from the effective radio ephemeris.

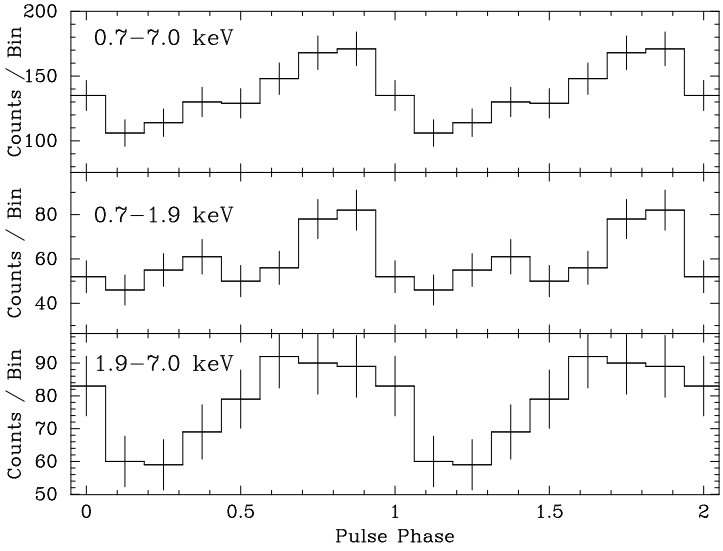

Fig. 2.— The folded pulse profiles are shown for the full energy range 0.7-7.0 (*top panel*) and two sub ranges 0.7-1.9 (*middle panel*) and 1.9-7.0 keV (*bottom panel*). The vertical axes show the number of events in each bin, and they are displayed so that the background levels correspond to the baseline of each panel. Two complete cycles are plotted for clarity.

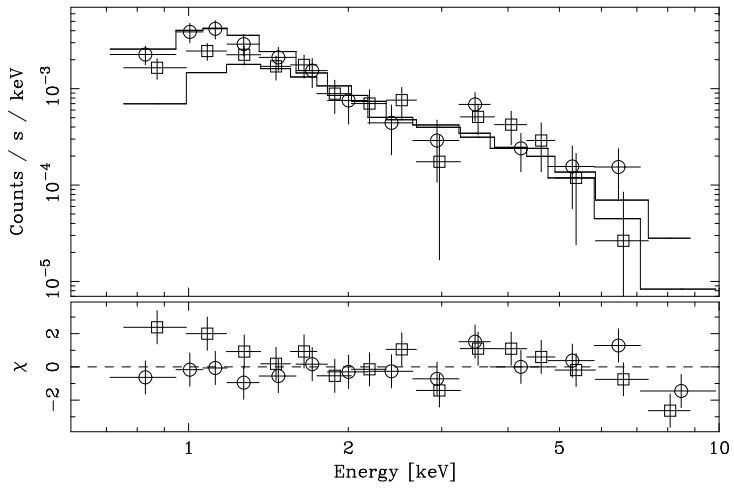

Fig. 3.— *Top panel*: The observed energy spectra and best-fit absorbed power-law function are shown for the two representative detectors. *Bottom panel*: Residuals normalized by the standard deviations are shown. Circles and squares show SIS1 and GIS3 data, respectively.